Temperature and Composition Dependence of the Interaction of δ-Lysin with Ternary Mixtures of Sphingomyelin/Cholesterol/POPC

Antje Pokorny,* Lindsay E. Yandek,* Adekunle I. Elegbede,† Anne Hinderliter,† and Paulo F. F. Almeida*
*Department of Chemistry and Biochemistry, University of North Carolina Wilmington, Wilmington, North Carolina; and
†Department of Pharmaceutical Sciences, North Dakota State University, Fargo, North Dakota

ABSTRACT The kinetics of carboxyfluorescein efflux induced by the amphipathic peptide δ-lysin from vesicles of porcine brain sphingomyelin (BSM), 1-palmitoyl-2-oleoyl-phosphatidylcholine (POPC), and cholesterol (Chol) were investigated as a function of temperature and composition. Sphingomyelin (SM)/Chol mixtures form a liquid-ordered (L_o) phase whereas POPC exists in the liquid-disordered (L_d) phase at ambient temperature. δ-Lysin binds strongly to L_d and poorly to L_o phase. In BSM/Chol/POPC vesicles the rate of carboxyfluorescein efflux induced by δ-lysin increases as the POPC content decreases. This is explained by the increase of δ-lysin concentration in L_d domains, which enhances membrane perturbation by the peptide. Phase separations in the micrometer scale have been observed by fluorescence microscopy in SM/Chol/POPC mixtures for some SM, though not for BSM. Thus, δ-lysin must detect heterogeneities (domains) in BSM/Chol/POPC on a much smaller scale. Advantage was taken of the inverse variation of the efflux rate with the L_d content of BSM/Chol/POPC vesicles to estimate the L_d fraction in those mixtures. These results were combined with differential scanning calorimetry to obtain the BSM/Chol/POPC phase diagram as a function of temperature.

INTRODUCTION

Over the past few years we have been examining the kinetics of carboxyfluorescein (CF) release from lipid vesicles induced by δ-lysin, a hemolytic, α-helical, amphipathic peptide secreted by *Staphylococcus aureus*. We have studied in detail the kinetics of the interaction of δ-lysin with large unilamellar vesicles (LUV) of 1-palmitoyl-2-oleoyl-phosphatidylcholine (POPC) and found that dye efflux from liquid-disordered (L_d) vesicles of pure POPC is caused by a rapid and transient translocation of a small peptide aggregate across the membrane (1,2). More recently, we examined the kinetics of CF release induced by δ-lysin from LUVs composed of ternary mixtures of sphingomyelin (SM), POPC, and cholesterol (Chol) at ambient temperature (3). That work led us to hypothesize that the rate of δ-lysin activity is dominated by the phase behavior of the membrane. Here, we examine the validity of this hypothesis by significantly extending the previous investigation to a broader range of lipid compositions and, especially, by including the effect of temperature (T) from 14 to 50°C. Ternary mixtures of SM, POPC, and Chol constitute a simple model of the outer leaflet of eukaryotic cell membranes. These mixtures have recently drawn a lot of attention because they also seem to embody the essential features of the lipid component of raft-containing membranes (4–8). An important finding regarding the interaction of δ-lysin with SM/Chol/POPC mixed vesicles at ambient temperature (3) is that the peptide shows a strong preferential partitioning (by a factor of $\sim 10^3$) into the L_d phase (POPC) relative to the liquid-ordered (L_o) phase (SM/Chol 1:1). Therefore, in a mixed SM/Chol/POPC bilayer containing L_d and L_o domains, δ-lysin interacts almost exclusively with the L_d domains, and the smaller the amount of L_d domains present, the faster the efflux (3). This occurs because with a smaller area of L_d domains, hence a higher peptide concentration therein, local membrane perturbation increases and peptide self-association is promoted (2). The observed rate of dye efflux is thus sensitive to the fraction of L_d phase present (3) and varies inversely with that fraction. Therefore, as will be shown here, information about the fractions of the L_d and L_o phases in the coexistence region can be directly obtained. Furthermore, because the domains must be large enough to be detected by the peptide, they are likely to be of order > 10 nm. This figure, however, is still much smaller than the resolution of fluorescence microscopy (order > 100 nm). Therefore, these experiments allow detection of domains on a different length scale, complementary to light-based microscopy. They also yield an estimate of the amounts of the two coexisting types of domains or phases, L_d and L_o.

Thus, δ-lysin can be used to probe the phase composition of SM/Chol/POPC bilayer membranes. Knowing the fractions of the L_d and L_o phases, the boundaries of the phase diagram can be estimated. The determination of phase diagrams of SM/Chol/POPC ternary systems has been a topic of great interest as they appear to contain regions of coexistence of two liquid phases believed to be relevant for the state of eukaryotic cell membranes, and also for the so-called lipid rafts (6,7,9–12). Coexistence of L_d and L_o phases was first proposed in theoretical work on binary mixtures of phosphatidylcholines (PC) and Chol (13,14). Subsequently, it was corroborated by several lines of experiments in binary (15–19) or ternary mixtures of two phospholipids and

Submitted March 12, 2006, and accepted for publication June 12, 2006.

Address reprint requests to P. F. Almeida, Tel.: 910-962-7300; E-mail: almeidap@uncw.edu.

0006-3495/06/09/2184/14 $2.00

doi: 10.1529/biophysj.106.085027

Chol (8,11,20–23). Lipid rafts (24,25) are thought to be protein/lipid domains rich in SM, Chol, glycosphingolipids, glycosylphosphatidylinositol-linked proteins, nonreceptor tyrosine kinases, and G-proteins (24–27). Rafts have been implicated in a number of cellular functions, including the facilitation of reactions between proteins and lipids that partition preferentially into the rafts, and sorting of components between different cell membranes (24). The current understanding of lipid rafts, liquid-ordered domains, or condensed complexes in biological and model membranes was the subject of several recent reviews (27–29). Initial evidence for the presence of rafts was obtained with classical detergent extraction, using Triton X-100 insolubility as a criterion (4,25,30). There is a correlation between formation of raftlike, liquid-ordered phases and detergent insolubility (4,30). Also, detergent extraction and fluorescence microscopy yield similar values for the partition coefficient of hydrophobic peptides between L_o and L_d phases (31,32). However, the question of the impact of detergent extraction on raft nature and composition still remains and it has been argued that the very process of detergent extraction may induce separation of raft lipids (33,34). Therefore, intense work has been dedicated to ascertain the existence of rafts in cell membranes. In particular, the determination of raft size and their visualization has received much attention (5,35). A difficulty in this regard is that lipid rafts are probably very dynamic structures (27,36,37).

In principle, phase diagrams can be determined using breaks in spectroscopic parameters of incorporated fluorescent probes or spin-labels. However, this may yield the phase boundaries but not the tie-lines, which, in a ternary system, have to be established independently to estimate the amounts of the coexisting phases. A phase diagram for palmitoyl-SM (PSM)/Chol/POPC has been published (6,38), with the suggestion of one tie-line. More recently, for dipalmitoylphosphatidylcholine (DPPC)/dioleoylphosphatidylcholine (DOPC)/Chol, tie-lines were obtained by a combination of fluorescence microscopy and ^{2}H-NMR spectroscopy (21), and a new method has been developed, using the DPPC/dilauroylphosphatidylcholine (DLPC)/Chol system, which allows for the determination of tie-lines using electron spin resonance (ESR) (22,23). In addition, phase diagrams for PSM/Chol/POPC and PSM/Chol/DOPC ternary systems have been proposed based on fluorescence microscopy (7), which include some indication of the tie-lines. However, significant disagreement exists between results from different groups (6,7), even in the placement of phase boundaries (see, for example, Fig. 2). This could be due, in part, to differences intrinsic to the methods used. For example, for domains to be visible by fluorescence microscopy, their size must be larger than the wavelength of the light used. In fact, fluorescence resonance energy transfer has indicated the existence of (small) domains that are not detected by fluorescence microscopy (8,38,39). Given these uncertainties and the relevance of the SM/Chol/POPC system for biological membranes, it is important to study the same system by different methods (21). This conclusion was also reached upon analysis of the state of knowledge of membrane microdomains (40). Here, we propose a phase diagram for SM/Chol/POPC as a function of temperature determined by an entirely different and novel approach. We hope that this will contribute to a better understanding of the matter at hand.

POPC was used as the unsaturated phospholipid because it seems the most biologically relevant choice (12). Porcine brain sphingomyelin (BSM) was used partly because it is more affordable than a pure SM. Of the available biological mixtures, this contains the largest amount of stearoyl (18:0) acyl chains (≈50%) and also a large fraction of nervonoyl (24:1) chains (≈20%). In general, the drawback of using a mixture as a pseudo-component in a mixed system is that further complexity can arise and the system is less pleasing from a pure physical chemical viewpoint. In its favor we should say that the sphingomyelin mixtures found in biological membranes may have unique properties not present in pure component sphingomyelins. This is inferred from differential scanning calorimetry (DSC) experiments that showed that a 1:1:1 mixture of 16:0-SM/18:0-SM/lignoceroyl(24:0)-SM exhibits a very cooperative melting behavior, with a transition width much narrower than expected from the individual heat capacity functions of the three separate components, and with a melting temperature (T_m) lower than any of the three (41). In fact, the mixture used in this article appears to follow the same trend, as shown below.

Finally, we place a word of caution on the use of terminology regarding the nature of inhomogeneities observed in these systems. Terms such as phases, domains, rafts, and condensed complexes have been used to describe regions of the membrane rich in ordered states of the phospholipids in mixtures with Chol (42). We will use the term ''phase'' in a generalized sense, to indicate that inhomogeneities are observed at some scale, macro- or microscopic. In some cases, when we feel the use of ''phase'' is least appropriate, the term ''domain'' will be preferred. But by using the terms domain or phase, we do not wish to imply any preconceived bias as to whether these heterogeneities are better described as phases, domains, or condensed complexes. This is simply a convenient way to refer to the inhomogeneity of these systems and, for consistency, we shall use the L_d/L_o terminology. If these domains were not phases in the thermodynamic limit, the use of phase diagrams (or of the term) may be legitimately questioned (7,9). However, a phase diagram can be simply viewed as a way of representing the different types of states present, such as different types of domains, which can still be treated in a rigorous manner by thermodynamics (and certainly by statistical mechanics) even if they are small (43). It is true, however, that small domains are subject to less strict thermodynamic constraints than macroscopic phases (9,43).

METHODS

Chemicals

1-Palmitoyl-2-oleoyl-*sn*-glycero-3-phosphocholine (POPC), in chloroform solution; porcine brain sphingomyelin (BSM), (2S,3R,4E)-2-acylamino-octadec-4-ene-3-hydroxy-1-phosphocholine, as powder or in chloroform solution; and cholesterol, as powder, were purchased from Avanti Polar Lipids (Alabaster, AL). The fatty acid chain composition of porcine brain sphingomyelin, specified by the vendor, is the following: 16:0 (2%), 18:0 (49%), 20:0 (5%), 22:0 (8%), 24:0 (6%), 24:1 (20%), and other chains (10%). Carboxyfluorescein (99% pure) was purchased from ACROS (Morris Plains, NJ). Organic solvents p.A. were purchased from Burdick & Jackson (Muskegon, MI). Lipids and probes were tested by TLC and used without further purification.

δ-Lysin

Formyl-NH-Met-Ala-Gln-Asp-Ile-Ile-Ser-Thr-Ile-Gly-Asp-Leu-Val-Lys-Trp-Ile-Ile-Asp-Thr-Val-Asn-Lys-Phe-Thr-Lys-Lys-COOH (δ-Lysin) was a gift from Dr. Birkbeck (University of Glasgow, Scotland). Its purification was described previously (1,44). For the dye efflux kinetics measurements, lyophilized δ-lysin was dissolved in distilled water acidified to pH $\simeq$ 3, to a final concentration of 200 μM as described before (3). Just before the kinetic experiments δ-lysin was diluted into 0.10 M KCl, pH 3.0. The low pH imparts the peptide with a net positive charge, which minimizes its aggregation.

Carboxyfluorescein efflux experiments

LUVs for CF efflux kinetics measurements were prepared by mixing the appropriate lipid amounts in 4:1 chloroform/methanol in a round bottom flask. The solvent was rapidly evaporated using a rotary evaporator (Büchi R-3000, Flawil, Switzerland) at 60–70°C. The lipid film was then placed under vacuum for 5–8 h and hydrated by the addition of buffer (20 mM MOPS pH 7.5, 0.1 mM EGTA, and 0.02% NaN_3, 50 mM CF) to give a final lipid concentration of 10 mM. The suspension of multilamellar vesicles was subjected to five freeze-thaw cycles to increase the degree of CF encapsulation. The suspension was then extruded 10 times through two stacked Nucleopore polycarbonate filters (Whatman, Florham, NJ) of 0.1-μm pore size, using a water-jacketed high pressure extruder from Lipex Biomembranes (Van couver, Canada) at 70°C. After extrusion, fluorophore-containing LUVs were passed through a Sephadex-G25 column (Sigma-Aldrich, St. Louis, MO) to separate the dye in the external buffer from the vesicles. The suspension was diluted in buffer to the desired lipid concentration and used for fluorescence measurements. The buffer used was 20 mM MOPS pH 7.5, containing 100 mM KCl, 0.1 mM EGTA, and 0.02% NaN_3, which has the same osmolarity as the CF-containing buffer. Lipid concentrations were assayed by the Bartlett phosphate method (45), modified as previously described (1), with the absorbance read at 580 nm. The kinetics of carboxyfluorescein efflux were recorded in a SLM-Aminco 8100 spectrofluorimeter (SLM-Aminco, Urbana, IL), adapted with a RX2000 rapid kinetics spectrometer accessory (Applied Photophysics, Leatherhead, UK), equipped with a RX pneumatic drive accessory (Applied Photophysics). The temperature was controlled to $\pm$0.1°C using a thermostated, circulating water bath (Thermo NESLAB, Newington, NH). CF efflux was measured by the relief of self-quenching of fluorescence, measured by excitation at 470 nm and emission at 520 nm. The peptide concentration was 0.5 μM in all experiments and the lipid concentration was 200 μM in all experiments, except for the data shown in Fig. 9.

Differential scanning calorimetry

Multilamellar vesicles (MLV) of lipid mixtures for DSC were prepared by aliquoting stock solutions of lipid in chloroform into borosilicate culture tubes using gas-tight syringes (Hamilton Company, Reno, NV). Phospholipid stock concentrations in chloroform were determined by phosphorus analysis (46). Samples were dried to a thin film under a stream of argon and placed on a high vacuum line overnight in the dark. Alternatively, the samples were lyophilized by briefly placing samples under vacuum to form a thin film of lipid, vented to argon upon removal from the vacuum, then dissolved in benzene/methanol (19:1, v/v), frozen in liquid N_2 and placed back under vacuum overnight, in the dark. Both types of samples were hydrated well above their transition temperature under argon in 20 mM MOPS pH 7.5, 100 mM KCl, 0.1 mM EGTA. The samples were slowly temperature-cycled through the main transition region of the SM twice, in the dark, before gently dispersing into a uniform suspension (to minimize introduction of oxygen). Samples were stored in the dark under argon and heated above the melting temperature of SM before being loaded into the calorimeter. Excess heat capacity functions of 10 mM MLV suspensions were obtained by heating at a scan rate of 10°C/h using MicroCal MC-2 and MicroCal VP-DSC instruments (Northampton, MA). Both sample preparation methods and calorimeters yielded the same melting and mixing behaviors as detected by DSC. The onset and completion temperatures of the gel-to-liquid crystalline phase transition were estimated as the two temperatures at which 5% and 95%, respectively, of the integral of the heat capacity curve are reached (47).

Preparation of red blood cell ghosts with encapsulated carboxyfluorescein

Red blood cell ghosts were prepared by the method of Dodge et al. (48). Briefly, the blood from a healthy donor was washed three times by centrifugation (at 600 $\times$ *g* for 15 min) and resuspended in isosmotic buffer (150 mM KCl, 10 mM MOPS, 0.1 mM EGTA, pH 7.5), at 4°C. CF was incorporated into the erythrocyte ghosts by hyposmotic shock with a large excess volume to yield a solution with the final composition of 10 mM CF, 20 mM KCl, 10 mM MOPS, pH 7.5. After the hyposmotic shock, the ghosts reseal entrapping CF. The dye left in the external medium was removed by gel filtration as described above.

Calculation of average relaxation times

The curves of carboxyfluorescein release as a function of time were characterized by a mean relaxation time (τ), as described before (3). Briefly, the mean relaxation time is obtained from the integral (49,50),

$$\tau = \frac{\int_0^\infty tf(t)dt}{\int_0^\infty f(t)dt}, \quad (1)$$

where

$$f(t) = \frac{dF(t)}{dt} \quad (2)$$

is the time-derivative of $F(t)$, which is the experimental curve of normalized fluorescence increase as a function of time. This curve increases as CF is released, until it essentially reaches a plateau (see Fig. 1). The time-derivative of $F(t)$, $f(t)$, behaves as the probability density function (49,50). For example, for a multiexponential decay, τ is the weighted average of the relaxation times of each exponential function. Before numerical differentiation the curves were smoothened as described before (3), to avoid errors due to experimental noise.

RESULTS

Effect of POPC content on dye efflux from L_d–L_o, mixed-phase vesicles of BSM/Chol/POPC at a constant temperature

The release of CF induced by δ-lysin is almost complete from pure POPC, L_d vesicles (Fig. 1, curve *A*), but very minor

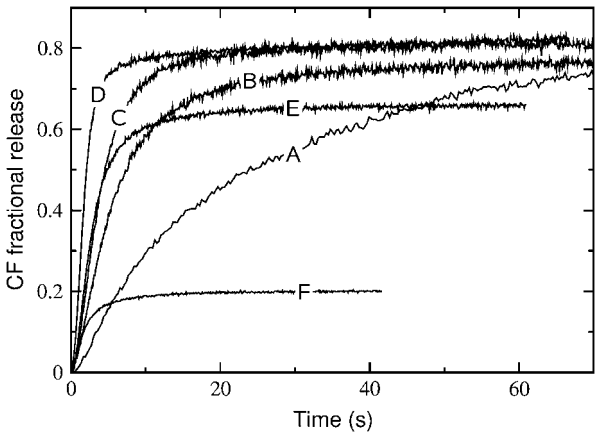

FIGURE 1 Carboxyfluorescein (CF) efflux induced by δ-lysin from lipid vesicles with the encapsulated dye at 38°C for various lipid compositions: (*A*) POPC; (*B*) BSM/Chol/POPC 10:10:80; (*C*) 15:15:70; (*D*) 30:30:40; (*E*) 40:40:20; and (*F*) BSM/Chol 50:50. In all experiments the peptide concentration was 0.5 μM and the lipid concentration was 200 μM.

from BSM/Chol 1:1, L_o vesicles (Fig. 1, curve *F*), at physiological temperature (38°C), at the same lipid and peptide concentrations, as shown before at ambient temperature (3). The small amount of CF efflux from BSM/Chol 1:1 is probably due to a small fraction of short or unsaturated chains present in this porcine brain sphingomyelin (BSM). Other authors have observed a residual disorder in bovine brain SM, which has similarly been attributed to a small fraction of low-melting chains (51). At ambient temperature (22°C), δ-lysin binds to the L_d phase (POPC) approximately three orders-of-magnitude better than to the L_o phase (SM/Chol 1:1) (3). In addition, the mean relaxation time, τ (defined by Eq. 1), for dye release increases with the POPC concentration in mixtures of BSM/Chol/POPC that exhibit nearly complete release. This is seen in the series of curves labeled *A*, *B*, *C*, and *D* in Fig. 1, where the POPC concentration is varied while keeping a constant, equimolar ratio of SM and Chol.

The combination of poor binding to and poor efflux across the L_o phase indicates that, in vesicles with L_d–L_o coexistence, dye efflux arises almost exclusively from peptides associated with the L_d domains. Furthermore, concentration of the peptide in L_d domains promotes the formation of δ-lysin aggregates, which are required for peptide translocation across the membrane, with concomitant CF efflux from the vesicle lumen (1,2). This is why, as the BSM/Chol content increases in BSM/Chol/POPC vesicles, CF-efflux time (τ) decreases (the rate increases) (Fig. 1), although the peptide does not bind strongly to, or release dye efficiently from BSM/Chol vesicles. That is, the smaller the amount of L_d phase present (POPC), the more efficient δ-lysin becomes in inducing CF efflux (3). In addition, at infinite time, close to 80% or more of the CF content of the vesicles is released as long as the amount of Chol is not too large (<40 mol %). But for BSM/Chol/POPC 4:4:2, the fraction of CF released drops, on average, to ≈50–60%, and for BSM/Chol 1:1, it is only ≈20%.

Temperature dependence of dye efflux from BSM/Chol/POPC vesicles

The kinetics of CF release from lipid vesicles, induced by δ-lysin, were measured as a function of temperature for: 1), pure POPC; 2), mixtures with equimolar ratios of BSM and Chol, with variable PC content, BSM/Chol/POPC 10:10:80, 15:15:70, 20:20:60, 25:25:50, 30:30:40, 40:40:20, and 50:50:0; and 3), BSM/Chol/POPC 10:30:60, 20:40:40, and 30:10:60. For easy reference, a Gibbs triangle indicating all the mixtures examined is shown in Fig. 2 (*circles* represent mixtures for which δ-lysin-induced efflux was measured; *squares* refer to calorimetric experiments). Also shown is the L_d–L_o coexistence region for PSM/Chol/POPC, as proposed by de Almeida et al. (6) (*solid line*) and Veatch and Keller (7) (*dashed line*). The phase diagram for BSM/Chol/POPC was not previously available, though some compositions were examined by Veatch and Keller (11), who did not detect macroscopic phase separation by fluorescence microscopy. In our work, the temperature was varied from 14 to 50°C. Table 1 shows the temperature-dependence of the mean relaxation time (τ, given by Eq. 1) of CF release curves for the mixtures that exhibit nearly complete dye release. The temperature-dependence is complex. Arrhenius plots corresponding to POPC vesicles and to two ternary mixtures are shown in Fig. 3. It is clear that CF efflux does not follow simple Arrhenius behavior, which would result in a straight line with negative slope in Fig. 3. At lower temperatures, τ is almost constant with temperature. At higher temperatures, the longer τ-values are probably a consequence of impaired

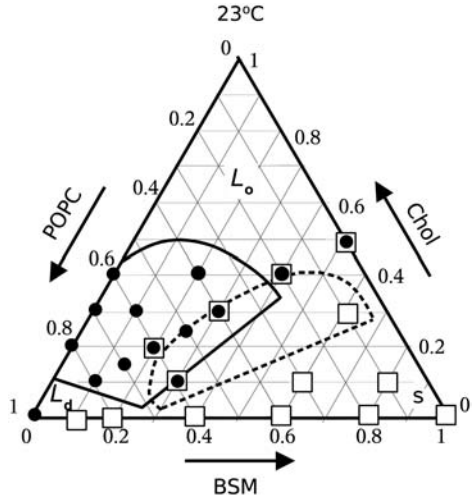

FIGURE 2 Gibbs triangle showing the compositions examined in this work by δ-lysin-induced dye release (*circles*) and DSC (*squares*). Also shown are the L_d–L_o coexistence regions from the phase diagram of PSM/Chol/POPC proposed by de Almeida et al. (6) (*solid lines*) and Veatch and Keller (7) (*dashed lines*), both at 23°C.

TABLE 1 Average relaxation time (τ) for the release of CF from vesicles of BSM/Chol/POPC

	Average relaxation time, τ (s)									
	SM/Chol/POPC mixtures							POPC/Chol mixtures		
T (°C)	10:10:80	15:15:70	20:20:60	25:25:50	30:30:40	10:30:60	30:10:60	80:20	70:30	60:40
14.0	17.1 ± 2.0	13.5 ± 0.3	9.0 ± 0.2	6.9 ± 0.6	9.9 ± 0.2	16.2 ± 0.2	25.6 ± 2.0	27 ± 1	23 ± 2	44 ± 4
18.0	19.3 ± 0.9	14.1 ± 2.2	7.2 ± 0.3	5.9 ± 0.5	6.1 ± 0.4	11.9 ± 0.4	14.3 ± 0.8	63 ± 6	20 ± 2	33 ± 3
22.0	20.7 ± 0.7	14.1 ± 2.6	6.9 ± 0.1	5.3 ± 0.4	5.6 ± 0.7	12.6 ± 1.7	10.9 ± 0.5	87 ± 9	28 ± 2	42 ± 5
26.0	26.6 ± 1.0	14.6 ± 3.5	6.5 ± 0.2	4.9 ± 0.4	4.1 ± 0.1	10.4 ± 0.2	8.4 ± 0.1	83 ± 2	26 ± 2	33 ± 4
30.0	26.5 ± 2.9	19.5 ± 3.0	6.8 ± 0.4	4.4 ± 0.3	3.8 ± 0.4	9.2 ± 0.2	8.7 ± 0.4	132 ± 10	67 ± 8	109 ± 8
34.0	26.8 ± 3.9	17.4 ± 2.2	7.5 ± 0.6	4.3 ± 0.3	3.4 ± 0.1	9.6 ± 0.1	8.9 ± 0.5	243 ± 17	168 ± 3	139 ± 12
38.0	34.7 ± 2.9	24.0 ± 2.0	9.2 ± 0.4	5.5 ± 0.2	3.3 ± 0.3	7.8 ± 0.2	11.3 ± 0.2	277 ± 15	320 ± 11	165 ± 8
42.0	53 ± 7	23.8 ± 4.4	14.9 ± 1.1	19 ± 5	3.2 ± 0.3	14.0 ± 0.2	17 ± 5	279 ± 25	274 ± 18	135 ± 4
46.0	141 ± 37	49 ± 9	38.0 ± 3.1	34 ± 10	4.8 ± 0.4	19 ± 1	45 ± 17	254 ± 29	148 ± 14	129 ± 16
50.0	173 ± 12	56.3 ± 0.8	48 ± 6	67 ± 17	7.5 ± 1.6	74 ± 9	72 ± 9	231 ± 22	268 ± 39	128 ± 17

The data represent average τ-values from, typically, three experimental dye efflux curves for each composition and temperature. The error bars are the corresponding standard deviations.

peptide binding due to partial unfolding, with loss of α-helical content and, consequently, amphipathicity. For all temperatures, the extent of CF release drops sharply at ≈40 mol % Chol, and becomes very small (≈20%) at 50 mol % Chol. We interpret this to mean that, at 40 mol % Chol, the amount of L_d phase present has become negligible or its domains are too small to be effectively detected by the peptide. Because the meaning of τ is not the same for mixtures that exhibit nearly complete release and for those that yield only limited dye release, τ-values were not calculated for the latter.

Dye efflux in POPC/Chol binary mixtures

We have also examined δ-lysin-induced efflux in three binary mixtures of POPC and Chol, with 20, 30, and 40 mol % Chol (Table 1, last three columns). At low temperatures, these measurements show that efflux from these POPC/Chol mixtures is very similar (if anything, slower) to efflux from pure POPC vesicles (Table 2, last column). This is in contrast to what is observed in BSM/Chol/POPC, where efflux is much faster than from pure POPC. This indicates that δ-lysin does not detect domains in POPC/Chol mixtures. Thus, we conclude that there is no coexistence region of L_d and L_o phases in the POPC/Chol binary system. However, small microdomains or fluctuations leading to appearance of L_o clusters cannot be excluded.

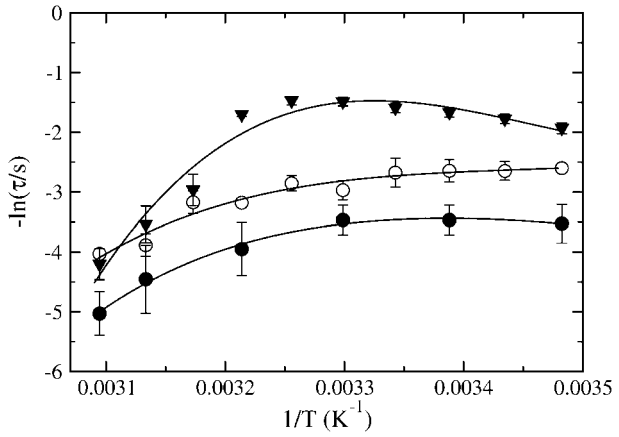

FIGURE 3 Arrhenius plot of the average relaxation time for dye efflux (τ) as a function of $1/T$. Simple Arrhenius behavior in this plot would yield a straight line with a negative slope. Data are shown for pure POPC (*solid circles*), and BSM/Chol/POPC 15:15:70 (*open circles*) and 25:25:50 (*solid triangles*). If not apparent, the error bars are inside the symbols. The lines are drawn only to guide the eye.

L_d and L_o fractions in BSM/Chol/POPC mixtures

It became apparent to us that the data shown in Table 1 could be used to obtain an estimate of the fractions of L_d and L_o domains coexisting in a BSM/Chol/POPC vesicle, provided a suitable calibration of the values of τ were available. To obtain such a calibration, the rates of dye efflux were measured in macroscopic mixtures of BSM/Chol (L_o) empty vesicles and POPC (L_d) vesicles loaded with CF, combined in proportions to span the range of the fractions of the two phases covered by the BSM/Chol/POPC mixtures examined, in the same temperature range (14–50°C). We refer to the τ of CF release in macroscopic mixtures of vesicles as a function of temperature as a calibration curve (Table 2). The idea is that τ for the macroscopic mixtures of vesicles should be the same as for the mixed-phase vesicles (co-lyophilized mixtures) if the fractions of L_d and L_o phases were the same in both. Therefore, given a certain average relaxation time τ for efflux in a mixed vesicle of BSM/Chol/POPC, the fraction of the L_d phase can be obtained from a comparison with a macroscopic mixture that gives that same τ. For example, at 30°C the mixture SM/Chol/POPC 15:15:70 yields a $\tau \simeq$ 20 s (Table 1). Using the calibration curve for this temperature (Fig. 4), we would estimate the amount of L_d phase in SM/Chol/POPC 15:15:70 to be 85%. The percentages of L_d phase calculated in this manner are shown in Table 3, which represents combined data using two independent

TABLE 2 Average relaxation time (τ) for the release of CF from macroscopic mixtures of BSM/Chol 1:1 vesicles and POPC vesicles

	Average relaxation time, τ (s)					
	% POPC in mixtures of SM/Chol 1:1 vesicles with POPC vesicles					
T (°C)	10%	20%	40%	60%	80%	100%
14.0	6.0 ± 1.6	7.2 ± 1.7	9.5 ± 3.6	14.3 ± 2.8	18 ± 6	34 ± 11
22.0	3.9 ± 0.9	4.8 ± 0.4	6.9 ± 0.9	12.1 ± 1.4	21 ± 3	31 ± 8
30.0	2.7 ± 0.4	3.2 ± 0.6	5.4 ± 1.1	9.7 ± 3.4	17 ± 4	32 ± 8
38.0	2.6 ± 0.8	2.6 ± 0.7	5.2 ± 0.7	8.3 ± 4.0	25 ± 16	52 ± 23
46.0	1.4 ± 0.4	2.3 ± 1.1	5.2 ± 2.1	18.5 ± 5.4	57 ± 28	86 ± 49
50.0	1.2 ± 0.3	2.2 ± 0.4	5.7 ± 1.0	26 ± 8	87 ± 29	153 ± 56

The data points represent average τ-values from typically six experimental dye efflux curves on two independent samples at each composition and temperature. The error bars are the corresponding standard deviations.

calibration curves. The percentage of L_d phase depends only weakly on temperature for most mixtures and increases with the POPC content, as expected. This is especially apparent in Fig. 5, where % L_d phase is plotted against the POPC content for that set of mixtures, for the various temperatures (indicated on Fig. 5). The % L_d phase increases almost linearly with POPC content for $T < 38$°C (*open symbols*). For $T \geq 42$°C (*solid symbols*), there is a sharp increase to ≈75% L_d phase at 50 mol % POPC, which stays level until 70 mol % POPC. Interestingly, 38°C (*hatched symbols*), which seems to be the transition between the two regimes, is approximately the T_m of BSM (Fig. 6). For the mixtures without equimolar amounts of SM and Chol, BSM/Chol/POPC 10:30:60 and 30:10:60, the % L_d phase remains in the vicinity of 60% (Table 3). Finally, the data for BSM/Chol/POPC 40:40:20 and 20:40:40 must be interpreted with caution because the final release is very incomplete (≈50% in both cases compared to ≥80% for the other mixtures). Therefore, we believe they correspond to regions of very small amount or very small domains of L_d phase. The estimates of the phase fractions thus obtained allow for some conclusions regarding the phase diagram of BSM/Chol/POPC. In addition, as described in the next sections, calorimetry was used to map the regions containing solid phase.

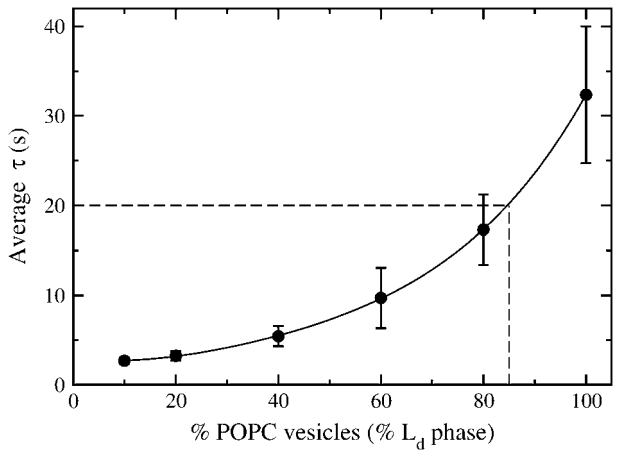

FIGURE 4 Example of the use of the calibration curve for a mixture of BSM/Chol/POPC 15:15:70 at 30°C. The measured $\tau \simeq 20$ s, which leads to an estimate of 85% L_d phase present in this mixture. The data is from Table 2, 30°C line.

DSC of BSM/POPC binary system

DSC was used to obtain the phase diagram for the BSM/POPC binary system. The DSC scans obtained for BSM and for BSM/POPC mixtures in the molar proportions of 8:2, 6:4, 4:6, 2:8, and 1:9 (*squares* in Fig. 2) are shown in Fig. 6 (in that order, from *top* to *bottom*). The main components of this BSM are acylated with stearoyl (18:0, 49%) or nervonoyl ($24{:}1^{\Delta 15c}$, 20%) chains. Other long saturated chains (20:0, 22:0, and 24:0) together account for ~20%. Stearoyl-SM has a melting temperature of 44°C from a nonannealed gel (52); nervonoyl-SM has a melting temperature of 27°C (53); the longer chain SM have similar melting temperatures: 45°C for 22:0-SM (53) and 49°C for 24:0-SM (41). The melting behavior of the BSM used here might therefore be expected to extend over a large temperature range. However, the experimental result reveals a significantly sharper melting, clustered at ~37°C (Fig. 6, *top curve*). This behavior is reminiscent of mixtures of 16:0-, 18:0-, and 24:0-SM, which exhibit a much more cooperative behavior than would be expected from the individual components (41), making it behave much more like a pure component than could be predicted a priori. The phase diagram for the BSM/POPC binary system, shown in Fig. 7, was generated from the DSC scans by assigning the onset and completion temperatures of the transitions to the points where the integral of the heat capacity curve reaches 5% and 95%, respectively, of the total integral (47). The approach of the DSC curves toward the baseline is asymptotic. In addition, there is always a certain amount of uncertainty in the baseline. Thus, particularly if the transition is broad, some uncertainty is always present in the assignment of the temperatures that mark the onset and completion of the phase transition. There are several standard methods commonly used, none of which is perfect: simulating the phase diagrams with regular solution theory; extrapolating linearly from the wings to the tails of the transition and taking the intersections as the onset and

TABLE 3 Percentage of L_d phase in vesicles of BSM/Chol/POPC as a function of temperature

	% L_d phase						
	SM/Chol/POPC mixtures						
T (°C)	10:10:80	15:15:70	20:20:60	25:25:50	30:30:40	10:30:60	30:10:60
14.0	74 ± 20	63 ± 27	37 ± 18	26 ± 23	41 ± 20	74 ± 19	90 ± 14
18.0	78 ± 9	65 ± 7	36 ± 12	25 ± 14	29 ± 13	57 ± 9	66 ± 8
22.0	80 ± 0	63 ± 4	40 ± 5	27 ± 10	30 ± 8	62 ± 2	57 ± 5
26.0	90 ± 5	67 ± 9	45 ± 7	30 ± 9	25 ± 7	57 ± 10	50 ± 8
30.0	94 ± 9	85 ± 7	45 ± 7	32 ± 9	27 ± 9	59 ± 13	57 ± 13
34.0	93 ± 10	81 ± 9	50 ± 0	34 ± 6	26 ± 9	56 ± 11	61 ± 11
38.0	90 ± 15	82 ± 17	62 ± 12	42 ± 5	27 ± 9	58 ± 14	70 ± 14
42.0	94 ± 9	76 ± 12	65 ± 7	71 ± 10	28 ± 8	64 ± 7	69 ± 9
46.0	100 ± 0	85 ± 21	78 ± 17	76 ± 15	37 ± 12	61 ± 7	85 ± 22
50.0	100 ± 0	75 ± 9	69 ± 2	79 ± 10	43 ± 2	82 ± 11	81 ± 10

The determination of % L_d phase was done separately for the two independent calibration curves and the estimated error is the standard deviation from the two estimates.

completion points; using some high order derivatives of the curve; or, as we have done, leaving out a small part of the curve integral on each side. We feel that our method is the most straightforward, makes the least assumptions, and immediately indicates the error involved—which is small. If 90% or 98% of the curve integral had been used instead of 95%, the onset and completion points would be very similar. We have used this approach several times in the past to obtain the onset and completion temperatures of the transition (47,54). The onset temperatures for mixtures with ≤40 mol % BSM were estimated to coincide with those of pure POPC.

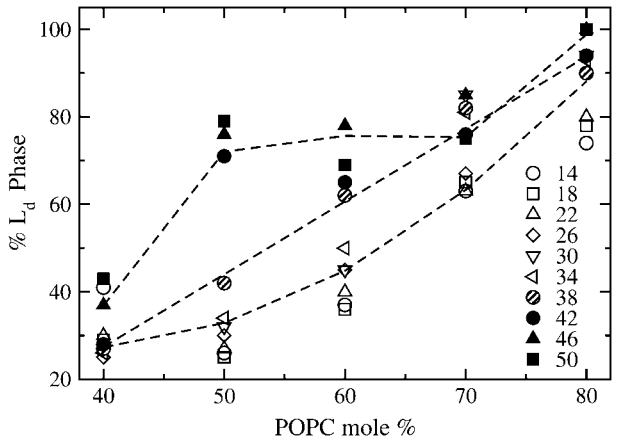

FIGURE 5 Percentage of L_d phase present in vesicles of BSM/Chol/POPC as a function of POPC content for the temperatures examined, which are indicated (in °C) on the figure. The open symbols are for $T < T_m$ of BSM, the hatched symbols are for 38°C ≈ T_m, and the solid symbols are for $T > T_m$ of BSM. The lines represent the average trend through each of the three types of points (*open*, *hatched*, and *solid*) and are drawn to guide the eye to the general behavior. The data are the same as in Table 3, but this plot emphasizes the close-to-linear dependence of the % L_d phase on POPC content for $T \leq T_m$, which is difficult to discern in Table 3.

DSC of BSM/Chol/POPC mixtures

DSC was used to further characterize the state of the BSM/Chol/POPC mixtures examined for CF efflux, as a means to detecting the presence of solid phase. Mixtures of BSM/Chol/POPC with the following molar ratios were examined: 1:1:0, 4:4:2, 3:3:4, 2:2:6, 8:1:1, 6:3:1, 6:1:3, and 3:1:6 (indicated by *squares* in Fig. 2). Most interesting, for the mixtures containing equimolar amounts of BSM and Chol no transition was observed between 3 and 80°C, independently of POPC content (not shown). This could be a consequence of a small heat and a very broad L_d/L_o transition preventing detection by DSC; or it could indicate that 1:1 may be a critical SM/Chol ratio. For the other mixtures, the DSC scans, shown in Fig. 8, reveal a complex heat capacity profile. Perhaps the most striking feature is that melting of these mixtures extends to higher temperatures than in BSM/POPC

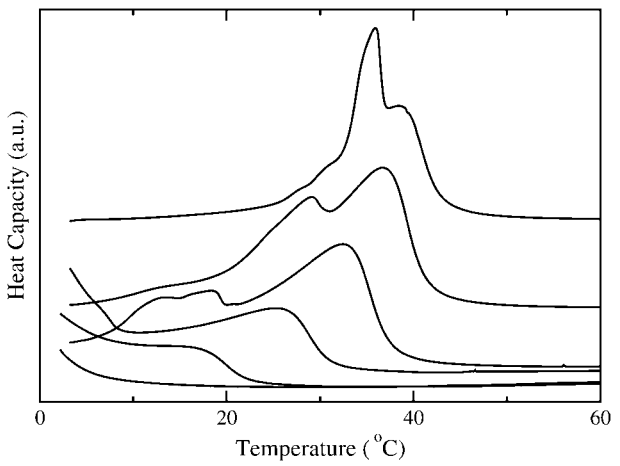

FIGURE 6 DSC scans of porcine brain sphingomyelin (BSM) and BSM/POPC MLVs (~100 mM lipid). (*Top* to *bottom*) BSM, and BSM/POPC 80:20, 60:40, 40:60, 20:80, and 10:90.

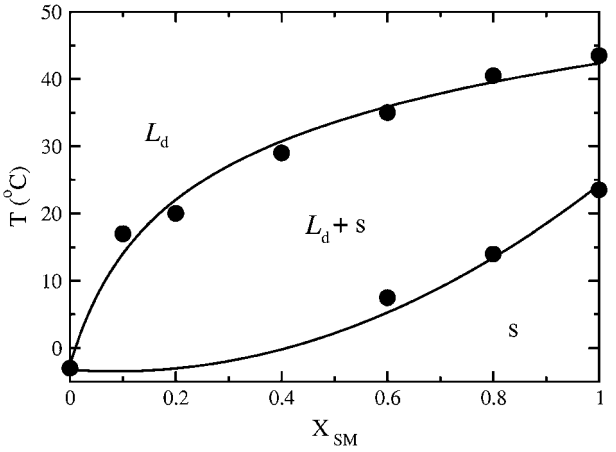

FIGURE 7 Phase diagram of BSM/POPC obtained from the DSC scans of Fig. 6. The onset and completion temperatures, defined as those points at which the integral of the heat capacity curve reaches 5 and 95% of its total value, are plotted against the mole fraction of BSM (X_{SM}). The regions of liquid-disordered (L_d), solid (s), and L_d–s coexistence are indicated.

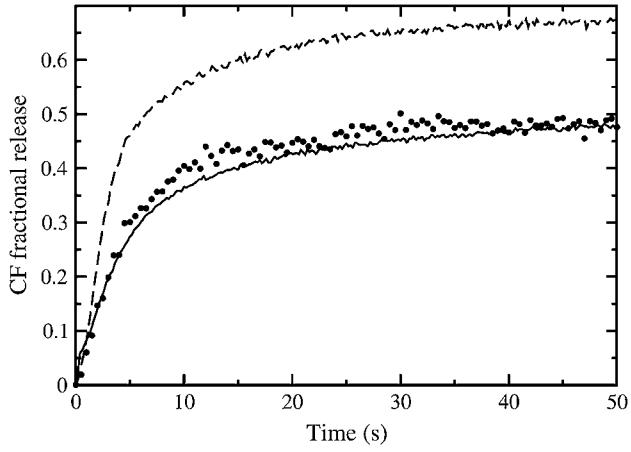

FIGURE 9 Carboxyfluorescein efflux from erythrocyte ghosts which were previously loaded with the dye by hyposmotic shock (*solid points*). The concentration of erythrocytes is estimated to be equivalent to 10–20 μM lipid LUVs. CF efflux curves from BSM/Chol/POPC 40:40:20 at lipid concentrations of 10 μM (*top*, *dashed curve*) and 25 μM (*bottom*, *solid curve*) are shown for comparison. The erythrocyte ghost efflux curve appears very similar to the 25 μM curve of BSM/Chol/POPC 40:40:20, both regarding the relaxation time and the total release of encapsulated dye. The δ-lysin concentration is 0.5 μM in all cases. The experiments were performed at room temperature.

mixtures and higher than BSM alone (Fig. 6), a feature that has been observed before (55).

Phase composition of human erythrocytes

Finally, as an illustration, δ-lysin was used to probe the L_d content of red blood cell membranes. Erythrocyte ghosts containing encapsulated CF were prepared by hyposmotic shock into a CF solution. Addition of δ-lysin revealed a low dye release (<50%), a pattern similar to mixtures with very low L_d content (Fig. 9). The CF-containing ghosts released CF similarly to the BSM/Chol/POPC 40:40:20 mixture. CF-release curves for BSM/Chol/POPC 40:40:20 with a concentration similar to that of the ghosts (10–20 μM) are also shown in Fig. 9. The similarities suggest that the red blood cell membrane is mainly in the L_o phase at ambient temperature. However, this result should be viewed more as an illustration because proteins in the ghost membrane could influence the observed behavior. This issue will be discussed in detail below.

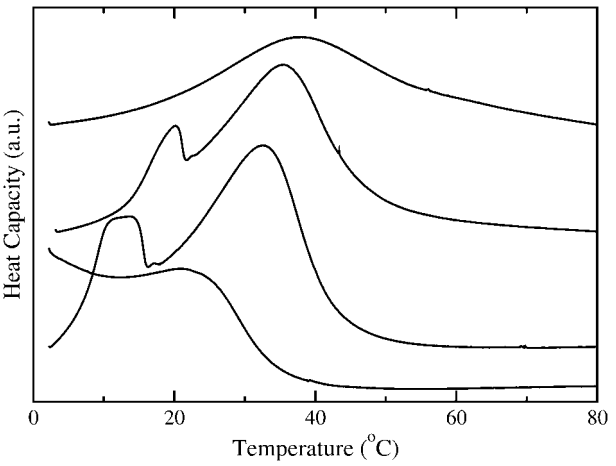

FIGURE 8 DSC scans of BSM/Chol/POPC mixtures with the molar compositions (from *top* to *bottom*): 60:30:10, 80:10:10, 60:10:30, and 30:10:60.

DISCUSSION

The main conclusion reached in this investigation is that the activity of the hemolytic, amphipathic, α-helical peptide δ-lysin is determined to a large extent by the phase behavior of the BSM/Chol/POPC ternary mixture, corroborating the initial hypothesis. However, the interpretation that is made here of the kinetics of dye efflux from mixed-phase vesicles induced by δ-lysin rests on a few important assumptions. Therefore, before discussing the results and using them to construct a phase diagram for the BSM/Chol/POPC ternary system as a function of temperature, it is important that those assumptions be made clear and their plausibility assessed. The three essential assumptions are that:

1. δ-Lysin partitions almost exclusively to the L_d phase in mixtures with L_d–L_o coexistence, regardless of temperature and composition.
2. The perturbation (which culminates with dye efflux) induced by the peptide on the L_d phase of two-phase, L_d/L_o vesicles is similar, in a first-order approximation, to the perturbation induced on pure L_d (POPC) vesicles, if the peptide concentration in the L_d phase is the same in both cases.

3. L_d/L_o interfaces do not have a major effect on the kinetics.

In addition to these assumptions, it is important to keep in mind the fact that the extent of dye efflux is very small (≈20%) from SM/Chol 1:1 at any temperature and, as a consequence, dye release occurs mostly across bilayer regions in the L_d state.

Assumption 1 is probably the easiest to justify. In fact, at room temperature, we have determined that the partition coefficient of δ-lysin is approximately three orders-of-magnitude in favor of the L_d phase when comparing SM/Chol 1:1 (L_o) with POPC (L_d) (3). It appears very unlikely that the change in temperature would alter the partition coefficient enough to render this assumption invalid, particularly if we take into account that the kinetics of CF efflux are only weakly dependent on temperature for a good part of the range spanned (Fig. 3 and Tables 1 and 2). Furthermore, preferential binding to the L_d phase appears to be a general feature of amphipathic peptides (56–58).

With regard to Assumption 2, it can be argued that because δ-lysin interacts with the system, as any probe does, it will alter that system. In this case, because the peptide partitions preferentially into the L_d phase it is expected to itself induce growth of the L_d at the expense of the L_o phase. This is certainly true as the system approaches equilibrium. However, it is reasonable to expect that the contribution of the initial state of the vesicles to the kinetics is dominated by the amount of L_d phase present and this parallels the contribution of the POPC vesicles in the macroscopic mixtures. The values of τ are not being interpreted here in an absolute manner, but used only in comparison with the macroscopic mixtures of vesicles and between the various vesicle compositions. Thus, this assumption appears safe because an erratic variation of the peptide behavior with composition is very unlikely. In addition, because the two phases, L_d and L_o, differ so much in their POPC content, there is not much room for increase of the L_d phase by extracting POPC from the L_o phase, where its amount is quite small. It is true that a probe (in this case, the peptide) always perturbs the system to some extent, but this is also true of lipid probes incorporated in the lipid membrane to begin with—and it has not prevented their extensive use in the determination of phase diagrams. It should also be noted that the amount of peptide used in our experiments is always very small, with a peptide/lipid ratio of 1:400. An advantage of the present method is that the initial state of the system is truly unperturbed by any probes.

Finally, with regard to Assumption 3, we have addressed this question before (3). It could be argued that L_d/L_o interfaces are defect lines, which could increase the rate of dye release. This is unlikely for three reasons. First, if defect lines existed, they should render mixed vesicles leaky even in the absence of peptide, but we do not observe this. Second, we have experimentally addressed the question of the role of interfaces in another system with L_d–L_o phase coexistence, dimyristoyl phosphatidylcholine/Chol (59). The rate of insertion of a small lipid amphiphile into vesicles with L_d–L_o coexistence was described exactly by additive contributions from insertion into L_d and L_o areas, without any increase in the rate due to the presence of interfaces (59). Third, if interfaces existed that increased the rate of δ-lysin-induced efflux this should be apparent as a minimum in τ as a function of increasing POPC content (increasing L_d phase) for each series of mixtures of BSM/Chol/POPC containing equimolar amounts of SM and Chol because the extent of interface should be maximal close to the point where the vesicles contain 50% of each phase. A pronounced maximum in the rate (minimum in τ) is the classical signature of the effect of interfaces in membrane permeability (60–62). However, as seen in the first five data columns of Table 1, no such minimum exists within experimental error, for any temperature with the possible exception of 14°C. Rather, τ decreases essentially monotonically with increasing POPC content at all temperatures. Therefore, if well-defined L_d/L_o interfaces exist, they are smooth, not defect lines. This observation may be of important biological significance.

If those assumptions are accepted, the data reported herein can be used to draw some important conclusions regarding the phase diagram of BSM/Chol/POPC. One downside of the method is its relatively low precision, which derives from the variation in the behavior of different vesicle preparations with regard to interaction with the peptide, leading to an average relative error of ≈25% in the estimate of the fraction of L_d phase (*error bars* in Table 3). However, the method has an asset also: using fluorescence microscopy alone, for example, domain structures below the limit of resolution appear as uniform. It has been pointed out that fluorescence resonance energy transfer indicates the existence of microdomains (8,38,39) in the same mixtures where fluorescence microscopy reveals uniform probe distributions. In addition, in a ternary system the fractions of the phases cannot be obtained from the phase boundaries without knowledge of the tie-lines. In our method, it is the fractions of the coexisting L_d and L_o phases that are directly estimated from the CF release data.

Use was made also of data on SM/Chol binary systems available in the literature. SM/Chol systems have been studied by ESR (17,63) and NMR (51), leading to somewhat different conclusions. ESR evidence clearly shows that SM/Chol membranes with high Chol content have ESR spectra typical of the L_o phase and, furthermore, that at intermediate Chol concentrations the ESR spectra are a superposition of spectra from L_d and L_o phases (63). In addition, measurements of lateral diffusion coefficients (D_L) in the SM/Chol-rich regions of SM/Chol/DOPC vesicles, yielded values of $D_L = 4.5 \times 10^{-9}$ cm^2 s^{-1} (64) and $D_L = 8 \times 10^{-9}$ cm^2 s^{-1} (65). These values are typical of the L_o-phase, not solid phases, indicating that the SM/Chol regions are in the L_o state. The ESR data are consistent with a L_d–L_o coexistence region above the T_m of the SM, between ~10 and 25 mol % Chol (17,63), whereas the NMR data place it between 15 and

50 mol % Chol (51). We have relied mostly on the ESR data to draw the phase boundaries in that part of the diagram, but this does not have a large influence, on the whole, on the ternary phase diagram proposed here.

The most important piece of information used was the estimate of the fractions of L_d phase obtained from the δ-lysin-induced CF release experiments, as a function of temperature (Table 3). The tie-lines were drawn in such a way as to maximize the agreement with the data of Table 3. This was combined with CF release data on POPC/Chol vesicles (Table 1), DSC data on BSM/Chol (Figs. 6 and 7), and BSM/Chol/POPC (Fig. 8), and literature data on SM/Chol systems. The general rules for the construction of ternary phase diagrams can be obtained from one of several standard references (66–69). The conclusions regarding the ternary phase diagram of BSM/Chol/POPC are summarized in Fig. 10 for three different temperatures, 22, 34, and 46°C. The tie-lines seem to run roughly parallel to a diagonal drawn from the POPC corner (*bottom left*) to the middle of the SM/Chol axis, and show a slight convergence toward that point. A comparison of the percentage of L_d phase obtained from the dye efflux experiments and calculated from the phase diagram proposed here is shown in Table 4. The agreement between experimental and calculated fractions is very good, consistent with the diagonal being a tie-line and with the location of the off-diagonal points, at compositions 10:30:60 and 30:10:60, both of which have ≈60% L_d phase (Table 3). These features of the L_d–L_o region resemble those of a theoretical phase diagram recently proposed for this type of system (70). The two ternary mixtures with compositions that exhibited a low final release, BSM/Chol/POPC 4:4:2 and 2:4:4, fall close to the phase boundaries of the phase diagram constructed using the other mixtures (Fig. 10). In our extensive experience with efflux kinetics of δ-lysin from POPC-based systems, with the lipid and peptide concentrations used here, if a sufficiently large fraction of L_d phase exists, CF release is always very close to complete (1–3) and a sharp decrease occurs at a well-defined POPC content (3). Therefore, we conjecture that mixtures with very incomplete release (≈50% or less) are likely to contain a negligible L_d phase fraction or very small L_d domains so that the peptide fails to detect them efficiently. In particular, the BSM/Chol/POPC 20:40:40 mixture appears to be close to the proposed location of a critical point (70).

The proposed phase diagram is qualitatively similar to those for other ternary mixtures containing cholesterol, SM/Chol/DOPC (7,10), and PSM/Chol/POPC (6,7), obtained using fluorescence microscopy and probes incorporated into those systems. It is also qualitatively similar to a recent ternary phase diagram calculated from a microscopic model (71). Quantitatively, however, our diagram is in better agreement with that of de Almeida et al. (6) than with that of Veatch and Keller (7) (compare Fig. 2 with the *left panel* of Fig. 10). The main difference with respect to the diagram of de Almeida et al. (6) is that those authors have included a L_d–L_o phase coexistence region for POPC/Chol binary

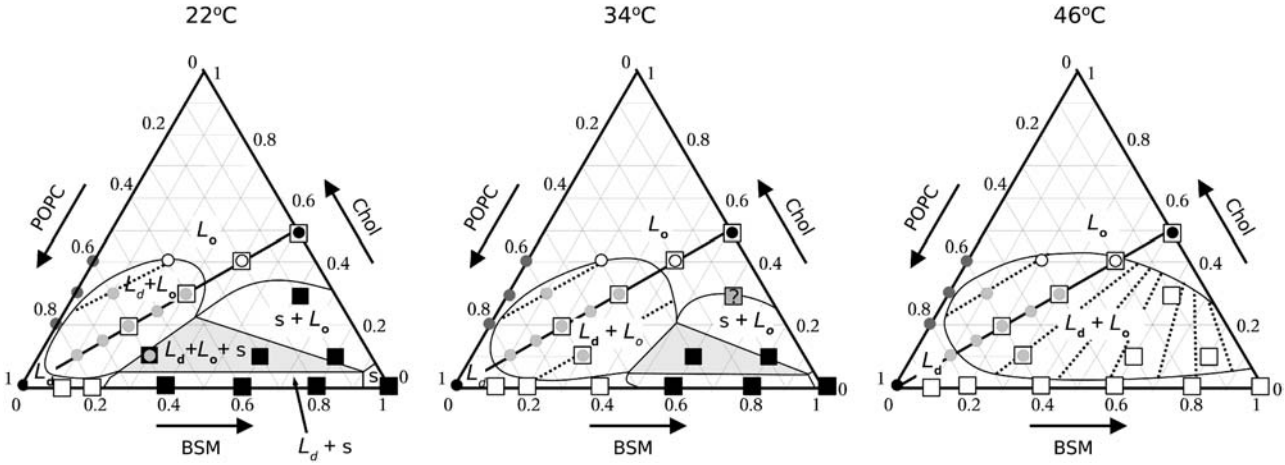

FIGURE 10 Ternary phase diagram of BSM/Chol/POPC at 22, 34, and 46°C constructed from CF efflux kinetics and DSC. Circles represent compositions examined by δ-lysin-induced CF efflux. The solid circles are the reference compositions (POPC and SM/Chol 1:1); the light shaded circles are compositions for which the L_d fractions were estimated from a comparison with macroscopic mixtures of the reference samples. Those L_d fractions are given in Table 4 (for the three temperatures shown). The tie-lines proposed represent the best match to those fractions taken globally (see Table 4). The open circles correspond to ternary mixtures that exhibited very incomplete CF release. The dark shaded circles represent mixtures of POPC/Chol examined, which showed no indication of phase separation as judged by dye release kinetics. The open squares represent mixtures examined by DSC but which show no gel present at that temperature. The shaded square represents a mixture for which we are uncertain regarding the existence of gel phase at 34°C. The solid squares represent mixtures in which gel exists at the temperature indicated. Mixtures on the diagonal (indicated by *open squares*) with compositions BSM/Chol/POPC 20:20:60, 30:30:40, 40:40:20, and BSM/Chol 50:50 were also examined by DSC but showed no transition. In the L_d–L_o coexistence region shown, the domains must be smaller than a few hundred nanometers because the compositions BSM/Chol/POPC 1:1:1, 1:1:2, and 2:1:2 do not exhibit macroscopic phase separation by fluorescence microscopy (11).

TABLE 4 Percentages of L_d phase in BSM/Chol/POPC mixtures obtained experimentally (*Exp*) and calculated (*Calc*) from the phase diagram for the three temperatures shown in Fig. 10

	22°C		34°C		46°C	
SM/Chol/POPC	Calc	Exp	Calc	Exp	Calc	Exp
10:10:80	81	80 ± 10	91	93 ± 10	100	100 ± 0
15:15:70	63	63 ± 4	75	81 ± 9	88	85 ± 21
20:20:60	48	40 ± 5	59	50 ± 0	72	78 ± 17
25:25:50	30	27 ± 10	43	34 ± 6	56	76 ± 15
30:30:40	13	30 ± 8	26	26 ± 9	37	37 ± 12
10:30:60	62	62 ± 2	54	56 ± 11	60	61 ± 7
30:10:60	62	57 ± 5	66	61 ± 11	81	85 ± 22

mixtures, based mainly on the observation of a multimodal distribution of lifetimes of the incorporated probe *trans*-parinaric acid and on a phase diagram proposed for POPC/Chol based on those types of data (72). This L_d–L_o phase coexistence region is not consistent with our dye efflux experiments in POPC/Chol mixtures for which τ is not smaller than from pure POPC (Tables 1 and 2). It is also not compatible with the orientation of the tie-lines in the L_d–L_o coexistence region (Fig. 10), which cannot intersect the POPC–Chol axis (66–69). The L_d–L_o region must, therefore, end before that. Drawing the tie-lines in a way that they asymptotically become parallel to the POPC–Chol axis is not consistent with the fractions of L_d and L_o phases inferred from CF efflux experiments (Table 3). It is possible that the discrepancies observed arise from the use of different sphingomyelins, BSM here and PSM in de Almeida et al. (6). However, a more likely explanation is that the lifetime distributions of *trans*-parinaric acid in POPC/Chol mixtures are due to small lipid clusters or fluctuations that are slower than the probe lifetime. This explanation is consistent with our placement of the boundary of the L_d–L_o coexistence region close to the POPC–Chol axis, suggesting that such fluctuations may be detected in POPC/Chol mixtures. The lack of L_d–L_o phase separation in POPC/Chol mixtures is in agreement with a recent study that used NMR and micromechanical measurements to come to that same conclusion (73). These authors also noted that fluctuations leading to the appearance of L_o microdomains cannot be excluded. It is also interesting that the same type of study by some of the same authors indicates the existence of phase separation in POPC/ergosterol (74). The end of the L_d–L_o coexistence region before the POPC–Chol axis is also a feature of the diagram proposed by Veatch and Keller (7), who used the exact same system as de Almeida et al. (6), but the extent of this region is larger in our diagram, intermediate between the two, but closer to de Almeida et al. (6) (compare Fig. 2 and Fig. 10, 22°C). This suggests that the differences observed in these phase diagrams reside not so much in the different sphingomyelins, but rather in the methods used. Thus, fluorescence microscopy detects only the largest domains, lifetime measurements detect also very small ones, and δ-lysin detects large and intermediate domains. In fact, Veatch and Keller (11) examined some compositions of BSM/Chol/POPC by fluorescence microscopy and found that mixtures of BSM/Chol/POPC 1:1:1, 1:1:2, and 2:1:2 do not exhibit phase separation on the micrometer scale (11). Yet, those compositions fall in the L_d–L_o coexistence region of our phase diagram (Fig. 10) at 34 and 46°C (at 22°C, the 1:1:1 and 2:1:2 mixtures are borderline). Again, we attribute this discrepancy to the difference in the sizes of domains detected by fluorescence microscopy (μm) and by δ-lysin. The domain size detected by the peptide must therefore be smaller than ≈100 nm, though probably not much smaller than the order of magnitude of peptide length, ~4 nm. Aussenac et al. (77) have used solid-state NMR to examine BSM/Chol/POPC mixtures. Based on the observation of a single quadrupolar splitting for the deuterated Chol, they suggested that Chol could be in fast exchange between two or more types of domains on the NMR timescale. With diffusion coefficients (D) of the order of 5×10^{-8} cm^2/s, and an NMR time $t \approx 10$ μs, this corresponds to an upper domain size of the order of $\sqrt{4Dt} \approx 10$ nm, similar to our suggestion.

CONCLUSION

We conclude by returning to the peptide activity and the relevance of the current results for biological membranes. The activity of δ-lysin toward membranes of BSM/Chol/POPC is largely determined by the phase behavior of the lipid vesicles. The temperature-dependence of the efflux kinetics does not follow Arrhenius behavior, but reflects the effect of temperature on the phase diagram, in particular on the amount of L_d phase present. As shown here, if the phase diagram is taken into account, an entirely self-consistent understanding of the kinetics of dye efflux is achieved. In the presence of L_d–L_o coexistence, δ-lysin partitions almost exclusively into the L_d domains (3). In this regard, to the best of our knowledge, it behaves similarly to all other amphipathic peptides that have been examined (56–58). The same is true in general for hydrophobic, transmembrane helices, which also prefer the L_d phase (31,32,56,75,76). The experiment reported here on efflux from erythrocyte ghosts suggests that the membrane of those cells is mainly in the L_o phase at ambient temperature, although this experiment should be regarded with some caution because of additional factors, such as binding of the peptide to membrane proteins, which

we cannot exclude. In fact, the composition of the outer leaflet of the erythrocyte membrane is closer to SM/Chol/PC 35:30:35 (78,79) than to 40:40:20, which is the composition that behaved similarly to the erythrocyte ghosts in the present experiments. This difference probably arises from the effect of proteins (≈50% of the membrane by weight) on the phase behavior of the erythrocyte ghost lipids or directly on δ-lysin. Nevertheless, the idea that mammalian plasma membranes are predominantly in the L_o phase was first suggested by Thewalt and Bloom (80). More recently, this was also suggested by Hao et al. (81), based on experimental evidence for several cell membranes, and yet again by McMullen et al. (12). If this is true, this study suggests that δ-lysin, which is a hemolytic peptide, may take advantage of this fact for enhanced activity against red blood cells by concentrating in the L_d phase. Of all mixtures examined here, BSM/Chol/POPC 30:30:40 is the closest to the composition of the outer leaflet of the erythrocyte membrane. It is interesting that this is the mixture against which δ-lysin is most effective (Table 1), with the shortest efflux times (τ), while still causing almost complete dye release. As also shown, BSM/Chol/POPC mixtures appear to be poised to change behavior close to 37°C (Fig. 5), which is approximately the T_m of BSM. This could represent a change in the connectivity of the L_d and L_o phases close to that temperature. Cells cannot, in general, change the temperature of their environment (thought the body can, in the case of fever, for example), but if they are poised close to a very responsive state, a change in the lipid or protein composition of their membrane may achieve a similar result. As recently argued (42), we concur with Hao et al. (81) and McMullen et al. (12) in that the current model for lipid rafts might need to be inverted: that the cell membrane is actually mainly in the L_o phase; that proteins partition preferentially into L_d domains, which are disconnected; that protein concentration in these domains may be important for function, for example in the formation of signaling complexes, just as originally proposed for rafts (24); and that, in some conditions, the cell may invert the domain connectivity (82). These ideas are largely speculative, but if correct, they could be extremely important for cell membrane function.

This work was supported in part by National Institutes of Health grants No. GM072507 (University of North Carolina Wilmington) and No. GM064443 (North Dakota State University).

REFERENCES

1. Pokorny, A., T. H. Birkbeck, and P. F. F. Almeida. 2002. Mechanism and kinetics of δ-lysin interaction with phospholipid vesicles. *Biochemistry*. 41:11044–11056.
2. Pokorny, A., and P. F. F. Almeida. 2004. Kinetics of dye efflux and lipid flip-flop induced by δ-lysin in phosphatidylcholine vesicles and the mechanism of graded release by amphipathic, α-helical peptides. *Biochemistry*. 43:8846–8857.
3. Pokorny, A., and P. F. F. Almeida. 2005. Permeabilization of raft-containing lipid vesicles by δ-lysin: a mechanism for cell sensitivity to cytotoxic peptides. *Biochemistry*. 44:9538–9544.
4. Ahmed, S. N., D. A. Brown, and E. London. 1997. On the origin of sphingolipid/cholesterol-rich detergent-insoluble cell membranes: physiological concentrations of cholesterol and sphingolipid induce formation of a detergent-insoluble, liquid-ordered lipid phase in model membranes. *Biochemistry*. 36:10944–10953.
5. Dietrich, C., L. A. Bagatolli, Z. N. Volovyk, N. L. Thompson, M. Levi, K. Jacobson, and E. Gratton. 2001. Lipid rafts reconstituted in model membranes. *Biophys. J.* 80:1417–1428.
6. de Almeida, R. F. M., A. Fedorov, and M. Prieto. 2003. Sphingomyelin/phosphatidylcholine/cholesterol phase diagram: boundaries and composition of lipid rafts. *Biophys. J.* 85:2406–2416.
7. Veatch, S. L., and S. L. Keller. 2005. Miscibility phase diagrams of giant vesicles containing sphingomyelin. *Phys. Rev. Lett.* 94:148101-1–148101-4.
8. Feigenson, G. W., and J. T. Buboltz. 2001. Ternary phase diagram of dipalmitoyl-PC/dilauroyl-PC/cholesterol: nanoscopic domain formation driven by cholesterol. *Biophys. J.* 80:2775–2788.
9. Veatch, S. L., and S. L. Keller. 2005. Seeing spots: complex phase behavior in simple membranes. *Biochim. Biophys. Acta*. 1746:172–185.
10. Smith, A. K., J. Buboltz, C. H. Spink, and G. W. Feigenson. 2003. Ternary phase diagram of the lipid mixture sphingomyelin/DOPC/cholesterol. *Biophys. J.* 84:372a.
11. Veatch, S. L., and S. L. Keller. 2003. Separation of liquid phases in giant vesicles of ternary mixtures of phospholipids and cholesterol. *Biophys. J.* 85:3074–3083.
12. McMullen, T. P. W., R. N. A. H. Lewis, and R. N. McElhaney. 2004. Cholesterol-phospholipid interactions, the liquid-ordered phase and lipid rafts in model and biological membranes. *Curr. Opin. Colloid Interface Sci.* 8:459–468.
13. Ipsen, J. H., G. Karlstroem, O. G. Mouritsen, H. Wennerstroem, and M. J. Zuckermann. 1987. Phase equilibria in the phosphatidylcholine-cholesterol system. *Biochim. Biophys. Acta*. 905:162–172.
14. Ipsen, J. H., O. G. Mouritsen, and M. J. Zuckermann. 1989. Theory of thermal anomalies in the specific heat of lipid bilayers containing cholesterol. *Biophys. J.* 56:661–667.
15. Vist, M. R., and J. H. Davis. 1990. Phase equilibria of cholesterol/dipalmitoylphosphatidylcholine mixtures: deuterium nuclear magnetic resonance and differential scanning calorimetry. *Biochemistry*. 29: 451–464.
16. Almeida, P. F. F., W. L. C. Vaz, and T. E. Thompson. 1992. Lateral diffusion in the liquid phases of dimyristoylphosphatidylcholine/cholesterol lipid bilayers: a free volume analysis. *Biochemistry*. 31: 6739–6747.
17. Sankaram, M. B., and T. E. Thompson. 1990. Interaction of cholesterol with various glycerophospholipids and sphingomyelin. *Biochemistry*. 29:10670–10675.
18. Sankaram, M. B., and T. E. Thompson. 1990. Modulation of phospholipid acyl chain order by cholesterol. A solid-state ^2H nuclear magnetic resonance study. *Biochemistry*. 29:10676–10684.
19. Sankaram, M. B., and T. E. Thompson. 1991. Cholesterol-induced fluid phase immiscibility in membranes. *Proc. Natl. Acad. Sci. USA*. 88:8686–8690.
20. Almeida, P. F. F., W. L. C. Vaz, and T. E. Thompson. 1993. Percolation and diffusion in three-component lipid bilayers: effect of cholesterol on an equimolar mixture of two phosphatidylcholines. *Biophys. J.* 64:399–412.
21. Veatch, S. L., I. V. Polozov, K. Gawrisch, and S. L. Keller. 2004. Liquid domains in vesicles investigated by NMR and fluorescence microscopy. *Biophys. J.* 86:2910–2922.
22. Chiang, Y. W., Y. Shimoyama, G. W. Feigenson, and J. H. Freed. 2004. Dynamic molecular structure of DPPC-DLPC-cholesterol ternary lipid system by spin-label electron spin resonance. *Biophys. J.* 87: 2483–2496.
23. Chiang, Y. W., J. Zhao, J. Wu, Y. Shimoyama, J. H. Freed, and G. W. Feigenson. 2005. New method for determining tie-lines in

coexisting membrane phases using spin-label ESR. *Biochim. Biophys. Acta.* 1668:99–105.

24. Simons, K., and E. Ikonen. 1997. Functional rafts in cell membranes. *Nature.* 387:569–572.
25. Brown, D. A., and E. London. 1998. Functions of lipid rafts in biological membranes. *Annu. Rev. Cell Dev. Biol.* 14:111–136.
26. Anderson, R. G., and K. Jacobson. 2002. A role for lipid shells in targeting proteins to caveolae, rafts, and other lipid domains. *Science.* 296:1821–1825.
27. Edidin, M. 2003. The state of lipid rafts: from model membranes to cells. *Annu. Rev. Biophys. Biomol. Struct.* 32:257–283.
28. McConnell, H. M., and M. Vrljic. 2003. Liquid-liquid immiscibility in membranes. *Annu. Rev. Biophys. Biomol. Struct.* 32:469–492.
29. Simons, K., and W. L. Vaz. 2004. Model systems, lipid rafts, and cell membranes. *Annu. Rev. Biophys. Biomol. Struct.* 33:269–295.
30. Brown, D. A., and E. London. 1997. Structure of detergent-resistant membrane domains: does phase separation occur in biological membranes? *Biochem. Biophys. Res. Comm.* 240:1–7.
31. McIntosh, T. J., A. Vidal, and S. A. Simon. 2003. Sorting of lipids and transmembrane peptides between detergent-soluble bilayers and detergent-resistant rafts. *Biophys. J.* 85:1656–1666.
32. Vidal, A., and T. J. McIntosh. 2005. Transbilayer peptide sorting between raft and nonraft bilayers: comparisons of detergent extraction and confocal microscopy. *Biophys. J.* 89:1102–1108.
33. Heerklotz, H. 2002. Triton promotes domain formation in lipid raft mixtures. *Biophys. J.* 83:2693–2701.
34. Keller, S., A. Tsamaloukas, and H. Heerklotz. 2005. A quantitative model describing the selective solubilization of membrane domains. *J. Am. Chem. Soc.* 127:11469–11476.
35. Samsonov, A. V., I. Mihalyov, and F. S. Cohen. 2001. Characterization of cholesterol-sphingomyelin domains and their dynamics in bilayer membranes. *Biophys. J.* 81:1486–1500.
36. Rietveld, A., and K. Simons. 1998. The differential miscibility of lipids as the basis for the formation of functional membrane rafts. *Biochim. Biophys. Acta.* 1376:467–479.
37. Young, R. M., D. Holowka, and B. Baird. 2003. A lipid raft environment enhances Lyn kinase activity by protecting the active site tyrosine from dephosphorylation. *J. Biol. Chem.* 278:20746–20752.
38. de Almeida, R. F. M., L. M. S. Loura, A. Fedorov, and M. Prieto. 2005. Lipid rafts have different sizes depending on membrane composition: a time-resolved fluorescence resonance energy transfer study. *J. Mol. Biol.* 346:1109–1120.
39. Silvius, J. R. 2003. Fluorescence energy transfer reveals microdomain formation at physiological temperatures in lipid mixtures modeling the outer leaflet of the plasma membrane. *Biophys. J.* 85:1034–1045.
40. Kenworthy, A. K. 2005. Where do we go from here? Meeting report on the Biophysical Society Discussion on ''Probing Membrane Microdomains'', October 28–31, 2004, Asilomar, CA. *Traffic.* 6:518–523.
41. Barenholz, Y., J. Suurkuusk, D. Mountcastle, T. E. Thompson, and R. L. Biltonen. 1976. A calorimetric study of the thermotropic behavior of aqueous dispersions of natural and synthetic sphingomyelins. *Biochemistry.* 15:2441–2447.
42. Almeida, P. F. F., A. Pokorny, and A. Hinderliter. 2005. Thermodynamics of membrane domains. *Biochim. Biophys. Acta.* 1720:1–13.
43. Hill, T. L. 1994. Thermodynamics of Small Systems (Parts I and II). Dover, New York, NY.
44. Birkbeck, T. H., and J. H. Freer. 1988. Purification and assay of staphylococcal δ-lysin. *Methods Enzymol.* 165:16–22.
45. Bartlett, G. R. 1959. Phosphorous assay in column chromatography. *J. Biol. Chem.* 234:466–468.
46. Kingsley, P. B., and G. W. Feigenson. 1979. The synthesis of a perdeuterated phospholipid: 1,2-dimyristoyl-*sn*-glycero-3-phosphocholine-d72. *Chem. Phys. Lipids.* 24:135–147.
47. Almeida, P. F. F., W. L. C. Vaz, and T. E. Thompson. 1992. Lateral diffusion and percolation in two-phase, two-component lipid bilayers. Topology of the solid phase domains in-plane and across the lipid bilayer. *Biochemistry.* 31:7198–7210.
48. Dodge, J. T., C. Mitchell, and D. J. Hanahan. 1963. The preparation and chemical characteristics of hemoglobin-free ghosts of human erythrocytes. *Arch. Biochem. Biophys.* 100:119–130.
49. Colquhoun, D. 1971. Lectures on Biostatistics. Clarendon Press, Oxford.
50. Colquhoun, D., and A. G. Hawkes. 1987,1994. The interpretation of single channel recordings. *In* Microelectrode Techniques. The Plymouth Workshop Handbook, 2nd Ed. D. Ogden, editor. The Company of Biologists Ltd., Cambridge, UK. 141–188.
51. Guo, W., V. Kurze, T. Huber, N. H. Afdhal, K. Beyer, and J. A. Hamilton. 2002. A solid-state NMR study of phospholipid-cholesterol interactions: sphingomyelin-cholesterol binary systems. *Biophys. J.* 83:1465–1478.
52. Estep, T. N., W. I. Calhoun, Y. Barenholz, R. L. Biltonen, G. G. Shipley, and T. E. Thompson. 1980. Evidence for metastability in stearoylsphingomyelin bilayers. *Biochemistry.* 19:20–24.
53. Cohen, R., Y. Barenholz, S. Gatt, and A. Dagan. 1984. Preparation and characterization of well defined *d*-erythro sphingomyelins. *Chem. Phys. Lipids.* 35:371–384.
54. Hinderliter, A. K., A. R. G. Dibble, R. L. Biltonen, and J. J. Sando. 1997. Activation of protein kinase C by coexisting diacylglycerol-enriched and diacylglycerol-poor lipid domains. *Biochemistry.* 36:6141–6148.
55. Calhoun, W. I., and G. G. Shipley. 1979. Sphingomyelin-lecithin bilayers and their interaction with cholesterol. *Biochemistry.* 18:1712–1722.
56. Gandhavadi, M., D. Allende, A. Vidal, S. A. Simon, and T. J. McIntosh. 2002. Structure, composition, and peptide binding properties of detergent soluble bilayers and detergent resistant rafts. *Biophys. J.* 82:1469–1482.
57. Epand, R. M., R. F. Epand, B. G. Sayer, G. Melacini, M. N. Palgulachari, J. P. Segrest, and G. M. Anantharamaiah. 2004. An apolipoprotein AI mimetic peptide: membrane interaction and the role of cholesterol. *Biochemistry.* 43:5073–5083.
58. Abraham, T., R. N. A. H. Lewis, R. S. Hodges, and R. N. McElhaney. 2005. Isothermal titration calorimetry studies of the binding of a rationally designed analogue of the antimicrobial peptide gramicidin S to phospholipid bilayer membranes. *Biochemistry.* 44:2103–2112.
59. Pokorny, A., P. F. F. Almeida, E. C. C. Melo, and W. L. C. Vaz. 2000. Kinetics of amphiphile association with two-phase lipid bilayer vesicles. *Biophys. J.* 78:267–280.
60. Clerc, S., and T. E. Thompson. 1995. Permeability of dimyristoylphosphatidylcholine/dipalmitoylphosphatidylcholine bilayer membranes with coexisting gel and liquid-crystalline phases. *Biophys. J.* 68:2333–2341.
61. Corvera, E., O. G. Mouritsen, M. A. Singer, and M. J. Zuckermann. 1992. The permeability and the effect of acyl-chain length for phospholipid bilayers containing cholesterol: theory and experiment. *Biochim. Biophys. Acta.* 1107:261–270.
62. Cruzeiro-Hansson, L., and O. G. Mouritson. 1988. Passive ion permeability of lipid membranes modelled via lipid-domain interfacial area. *Biochim. Biophys. Acta.* 944:63–72.
63. Collado, M. I., F. M. Goñi, A. Alonso, and D. Marsh. 2005. Domain formation in sphingomyelin/cholesterol mixed membranes studied by spin-label electron spin resonance spectroscopy. *Biochemistry.* 44: 4911–4918.
64. Bacia, K., D. Scherfeld, N. Kahya, and P. Schwille. 2004. Fluorescence correlation spectroscopy relates rafts in model and native membranes. *Biophys. J.* 87:1034–1043.
65. Kahya, N., D. Scherfeld, K. Bacia, B. Poolman, and P. Schwille. 2003. Probing lipid mobility of raft-exhibiting model membranes by fluorescence correlation spectroscopy. *J. Biol. Chem.* 278:28109–28115.
66. Findlay, A. 1951. The Phase Rule, 9th Ed. Dover, New York, NY.

67. Rhines, F. N. 1956. Phase Diagrams in Metallurgy. Their Development and Application. McGraw-Hill, New York, NY.

68. Prince, A. 1966. Alloy Phase Equilibria. Elsevier, New York, NY.

69. Yeh, H. C. 1970. Interpretation of phase diagrams. *In* Phase Diagrams. Materials Science and Technology, Vol. I. A. M. Alper, editor. Academic Press, New York, NY. 167–197.

70. McConnell, H. 2005. Complexes in ternary cholesterol-phospholipid mixtures. *Biophys. J.* 88:L23–L25.

71. Elliott, R., I. Szleifer, and M. Schick. 2006. Phase diagram of a ternary mixture of cholesterol and saturated and unsaturated lipids calculated from a microscopic model. *Phys. Rev. Lett.* 96:098101–1-098101–4.

72. Mateo, R. C., A. U. Acuña, and J.-C. Brochon. 1995. Liquid-crystalline phases of cholesterol/lipid bilayers as revealed by the fluorescence of *trans*-parinaric acid. *Biophys. J.* 68:978–987.

73. Henriksen, J., A. C. Rowat, E. Brief, Y. W. Hsueh, J. L. Thewalt, M. J. Zuckermann, and J. H. Ipsen. 2006. Universal behavior of membranes with sterols. *Biophys. J.* 90:1639–1649.

74. Hsueh, Y.-W., M.-T. Chan, P. Patty, C. Code, J. Cheng, B. Frisken, M. J. Zuckermann, and J. Thewalt. 2006. The physical properties of POPC-sterol membranes: a deuterium NMR and lysis tension study. *Biophys. J.* 90:1047–Pos.

75. Bacia, K., C. G. Schuette, N. Kahya, R. Jahn, and P. Schwille. 2004. SNAREs prefer liquid-disordered over ''raft'' (liquid-ordered) domains when reconstituted into giant unilamellar vesicles. *J. Biol. Chem.* 279:37951–37955.

76. Fastenberg, M. E., H. Shogomori, X. Xu, D. A. Brown, and E. London. 2003. Exclusion of a transmembrane-type peptide from ordered-lipid domains (rafts) detected by fluorescence quenching: extension of quenching analysis to account for the effects of domain size and domain boundaries. *Biochemistry.* 42:12376–12390.

77. Aussenac, F., M. Tavares, and E. J. DuFourc. 2003. Cholesterol dynamics in membranes of raft composition: a molecular point of view from ^{2}H and ^{31}P solid-state NMR. *Biochemistry.* 42:1383–1390.

78. Cullis, P. R., and M. J. Hope. 1985. Physical properties and functional roles of lipids in membranes. *In* Biochemistry of Lipids and Membranes. D. E. Vance and J. E. Vance, editors. Benjamin/Cummings, Menlo Park, CA.

79. Zachowski, A. 1993. Phospholipids in animal eukaryotic membranes: transverse asymmetry and movement. *Biochem. J.* 234:1–14.

80. Thewalt, J. L., and M. Bloom. 1992. Phosphatidylcholine:cholesterol phase diagrams. *Biophys. J.* 63:1176–1181.

81. Hao, M., S. Mukherjee, and F. R. Maxfield. 2001. Cholesterol depletion induces large-scale domain segregation in living cell membranes. *Proc. Natl. Acad. Sci. USA.* 98:13072–13077.

82. Thompson, T. E., M. B. Sankaram, R. L. Biltonen, D. Marsh, and W. L. C. Vaz. 1995. Effects of domain structure on in-plane reactions and interactions. *Mol. Membr. Biol.* 12:157–162.